



Design, synthesis and biological evaluation of novel 5-phenyl-1*H*-pyrazole derivatives as potential BRAF^{V600E} inhibitors



Shu-Fu Wang[†], Yin-Ling Zhu[†], Ping-Ting Zhu, Jigar A. Makawana, Ya-Liang Zhang, Meng-Yue Zhao, Peng-Cheng Lv^{*}, Hai-Liang Zhu^{*}

State Key Laboratory of Pharmaceutical Biotechnology, Nanjing University, Nanjing 210093, People's Republic of China

ARTICLE INFO

Article history:

Received 6 June 2014

Revised 31 July 2014

Accepted 21 August 2014

Available online 6 September 2014

Keywords:

BRAF^{V600E} inhibitor

Pyrazole

Niacinamide

Molecular docking

3D-QSAR

ABSTRACT

A series of novel 5-phenyl-1*H*-pyrazole derivatives (**5a–5u**) containing niacinamide moiety were synthesized and evaluated for biological activity as potential BRAF^{V600E} inhibitors. Among them, compound **5h** exhibited the most potent inhibitory activity with an IC₅₀ value of 0.33 μM for BRAF^{V600E}. Antiproliferative assay results indicated that compound **5h** has better antiproliferative activity against WM266.4 and A375 in vitro with IC₅₀ value of 2.63 and 3.16 μM, respectively, being comparable with the positive control vemurafenib. Molecular docking of **5h** into the BRAF^{V600E} active site was performed to determine the probable binding mode. Furthermore, molecular docking and 3D QSAR study by means of DS 3.5 (Discovery Studio 3.5, Accelrys, Co. Ltd) explored the binding modes and the structure and activity relationship (SAR) of these derivatives.

© 2014 Published by Elsevier Ltd.

1. Introduction

The RAS–RAF–MEK–ERK signaling pathway plays a critical role in human oncogenesis.^{1–3} It normally acts as a medium to transduce signals from cell surface receptors to the nucleus and give rise to the expression of genes that regulate cell growth, survival and differentiation.² The RAS will be activated when an extracellular signal molecule binds to its membrane receptor. One main effector of RAS is the RAF family proteins, a series of cytoplasmic serine/threonine protein kinases, which is composed of A-RAF, B-RAF, and C-RAF (also known as RAF-1).^{4–7} It mediates intracellular signal transduction by the phosphorylation and activation of MEKs after which the downstream kinases, extracellular signal-regulated kinases (ERKs), were triggered.⁸ Phosphorylated products of ERKs are some transcription factors which directly or indirectly regulate gene expression, cytoskeleton construction, cause prevention of apoptosis, cell cycle arrest and contribute to tumorigenesis. Therefore, kinase of this pathway such as RAF can serve as a promising therapeutic target for anticancer drug development.

Among the RAF family proteins, B-RAF has more biochemical potencies than A-RAF and C-RAF because it is easier to be activated.⁹ Up to now, a great number of activating mutations have been detected in B-RAF gene, but the most common B-RAF mutation in

human cancer is a single base substitution at nucleotide 600 which converts a valine to a glutamic acid (V600E; formally identified as V599E).¹⁰ This single mutation leads to constitutive activation of B-RAF, independent of RAS function, resulting in unremitting proliferation of cancer cells.¹¹ Mutations in B-RAF have been detected in approximately 8% of human tumors, melanomas (50%), thyroid cancers (30–70%), serous low-grade ovarian cancers (30%) and colorectal cancers (10%).^{11,12}

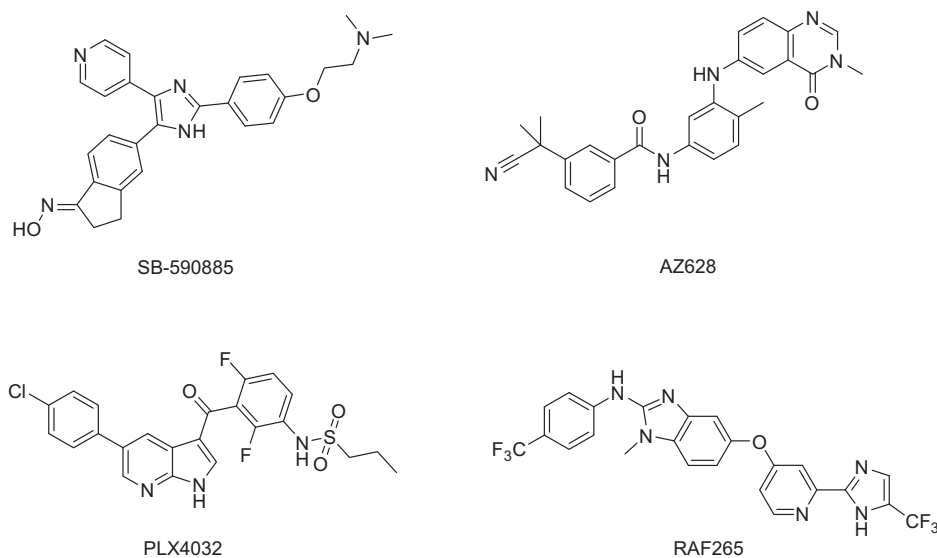
Inhibitors targeting BRAF have been developed such as SB-590885, AZ628, RAF265 and PLX4032 (vemurafenib)^{13–16} (Scheme 1). Among of these, PLX4032 is a highly specific BRAF^{V600E} inhibitor that binds preferentially to the active conformation of the kinase.¹⁷ It employs a common scaffold that includes a *meta* or *para* substituted aromatic system inserting into the lipophilic DFG-out pocket and a terminal aromatic group (phenyl or pyrazole) that fills the allosteric pockets created by the displacement of the DFG loop. A linker is needed to interact with the salt bridge formed between residues Glu501 and Lys483.¹⁸

Pyrazole derivatives are widely used in medicine research for their officinal potencies such as antitumor, anti-inflammatory, antibacterial, analgesic, fungistatic, and anti-hyperglycemic.^{19–22} GDC-0879 contained the pyrazole ring is a highly selective and potent RAF small-molecule inhibitor that can inhibit BRAF^{V600E} kinase activity with K_i of 0.13 nM.²³ In addition, nicotinamide, which has various pharmacological effects when doses in excess of nutritional requirements are given, is known as a radiation sensitizer and used clinically in cancer therapy.^{24,25} Its analogues were

* Corresponding authors. Tel.: +86 25 83592572; fax: +86 25 83592672.

E-mail address: zhuhl@nju.edu.cn (H.-L. Zhu).

[†] These authors contributed equally to this work.



Scheme 1. Chemical structures of antitumor agents and lead BRAF^{V600E} inhibitors.

found to induce an efficient and specific inactivation of the exogenous transforming genes such as RAF.²⁶ Recently, compounds contained niacinamide moiety have been synthesized and showed greater BRAF^{V600E} inhibitory activity.^{27,28}

Recent years, our group have reported a number of novel pyrazol derivatives as potent inhibitors targeting BRAF and some of them showed potent antitumor activity.^{29–31} Based on the statements above and to extend our research, a series of 5-phenyl-1*H*-pyrazole derivatives contained niacinamide moiety were designed and synthesized. Upon biological evaluation, some of the synthesized compounds were found as potent inhibitors of BRAF^{V600E}. Docking simulation was performed using the X-ray crystallographic structure of BRAF^{V600E} in complex with the most potent inhibitor to explore the binding mode of the compound at the active site. Furthermore, QSAR model was built to study the structure–activity relationship that guides the further study.

2. Results and discussion

2.1. Chemistry

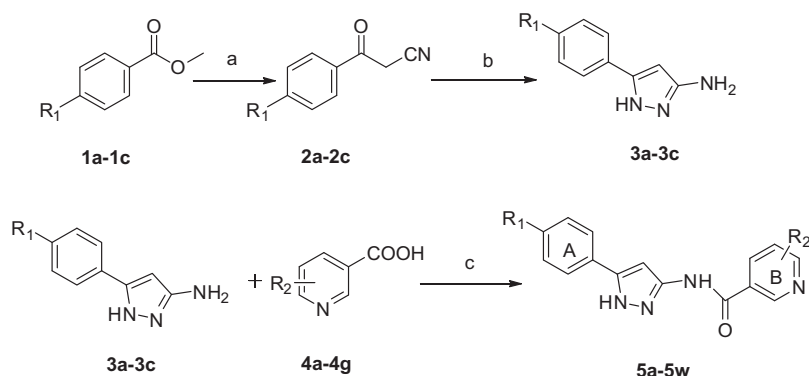
The general synthesis of pyrazol derivatives is outlined in Scheme 2. First of all, **2a–2c** were synthesized in THF by treating *p*-substituted methyl benzoate with acetonitrile using NaH as

catalyst. Secondly, compounds **2a–2c** and hydrazine hydrate were dissolved in ethanol and refluxed for 1 h to get compounds **3a–3c**. Lastly, the coupling reaction between the obtained compounds **3a–3c** and nicotinic acids was performed by using 1-ethyl-3-(3-dimethylaminopropyl)carbodiimide hydrochloride (EDCI) and *N*-hydroxybenzotriazole (HOBT) in anhydrous methylene dichloride under reflux condition to get the desired compounds **5a–5u**. All synthesized compounds were given satisfactory analytical and spectroscopic data which were in full accordance with their depicted structures.

2.2. Biological activity

2.2.1. Antiproliferative activity

To test the anticancer activities of the synthesized compounds, we evaluated antiproliferative activities of compounds **5a–5u** against BRAF^{V600E} cell lines (WM266.4 and A375) and wild type BRAF cell line (WM1361). The results were summarized in Table 1. 5-Phenyl-1*H*-pyrazole derivatives beared niacinamide moiety showed remarkable antiproliferative effects on the BRAF^{V600E} cell lines. Among them, compound **5h** displayed the most potent inhibitory activity (IC₅₀ = 2.63 μM for WM266.4 and IC₅₀ = 3.16 μM for A375) which was compared to the positive control vemurafenib (IC₅₀ = 0.06 μM for WM266.4 and IC₅₀ = 0.19 μM for



Scheme 2. General synthesis of 5-phenyl-1*H*-pyrazole derivatives (**5a–5u**). Reagents and conditions: (a) CH₃CN, NaH, THF, reflux, 4 h; (b) NH₂NH₂·H₂O, CH₃SO₃H, EtOH, reflux, 1 h; (c) EDCI, HOBT, dichloromethane, reflux, 1 h.

Table 1
Structural features, inhibition (IC₅₀) of WM266.4, A375 and WM1361 cells proliferation by compounds **5a–5u**

Compound	R ₁	R ₂	IC ₅₀ ± SD (μM)		
			WM266.4 ^a	A375 ^a	WM1361 ^b
5a	H	2-F	3.77 ± 0.75	4.88 ± 0.74	14.55 ± 0.44
5b	H	2-Cl	6.22 ± 0.56	7.34 ± 0.85	17.34 ± 0.56
5c	H	2-OCH ₃	8.75 ± 0.32	9.94 ± 1.02	25.77 ± 0.27
5d	H	5-Br	6.88 ± 0.86	8.12 ± 1.24	19.28 ± 0.68
5e	H	6-Br	6.73 ± 1.02	8.87 ± 0.98	19.43 ± 0.66
5f	H	6-Cl	6.43 ± 0.55	7.85 ± 0.85	18.98 ± 0.31
5g	H	6-OCH ₃	8.48 ± 0.58	9.56 ± 0.64	24.65 ± 0.46
5h	Br	2-F	2.63 ± 0.84	3.16 ± 0.84	13.25 ± 0.55
5i	Br	2-Cl	5.35 ± 0.36	6.44 ± 0.75	15.77 ± 0.68
5j	Br	2-OCH ₃	7.76 ± 0.45	8.73 ± 0.35	25.78 ± 0.34
5k	Br	5-Br	6.45 ± 0.48	7.05 ± 0.49	17.87 ± 0.25
5l	Br	6-Br	6.78 ± 0.62	7.67 ± 0.73	18.56 ± 0.64
5m	Br	6-Cl	5.72 ± 0.26	6.88 ± 0.55	16.74 ± 0.39
5n	Br	6-OCH ₃	7.35 ± 0.37	8.42 ± 0.64	24.86 ± 0.41
5o	CH ₃	2-F	4.68 ± 1.22	5.42 ± 0.28	15.66 ± 0.68
5p	CH ₃	2-Cl	6.99 ± 0.54	8.22 ± 0.37	18.45 ± 0.46
5q	CH ₃	2-OCH ₃	10.25 ± 0.62	11.12 ± 0.64	30.98 ± 1.05
5r	CH ₃	5-Br	8.23 ± 0.27	9.42 ± 0.56	20.34 ± 0.34
5s	CH ₃	6-Br	8.56 ± 0.88	9.91 ± 0.24	20.56 ± 1.22
5t	CH ₃	6-Cl	7.47 ± 0.71	8.89 ± 0.29	19.33 ± 0.65
5u	CH ₃	6-OCH ₃	9.12 ± 0.24	8.95 ± 0.69	28.45 ± 0.94
Vemurafenib ^c			0.06 ± 0.008	0.19 ± 0.02	1.87 ± 0.15

^a BRAF^{V600E} cell lines.

^b Wild type BRAF cell line.

^c Used as a positive control.

A375, respectively). Also, the compounds showed better inhibitory activity to BRAF^{V600E} cell lines (WM266.4 and A375) than to wild type BRAF cell line (WM1361).

2.2.2. BRAF inhibitory activity

The BRAF^{V600E} kinases inhibitory potency of the synthesized pyrazole derivatives was examined using a solid-phase ELISA assay and the results were summarized in Table 2. All of the tested compounds showed potent BRAF^{V600E} kinases inhibitory activities with IC₅₀ values between 0.33 and 1.88 μM. Among them, compound **5h** displayed the most potent anti-BRAF^{V600E} kinase activity with IC₅₀ of 0.33 μM.

Table 2
BRAF^{V600E} inhibitory activity of synthetic compounds

Compound	R ₁	R ₂	IC ₅₀ ± SD (μM)
5a	H	2-F	0.56 ± 0.63
5b	H	2-Cl	0.75 ± 0.55
5c	H	2-OCH ₃	1.54 ± 0.36
5d	H	5-Br	0.98 ± 0.64
5e	H	6-Br	1.21 ± 0.27
5f	H	6-Cl	0.84 ± 0.82
5g	H	6-OCH ₃	1.50 ± 0.23
5h	Br	2-F	0.33 ± 0.35
5i	Br	2-Cl	0.69 ± 0.44
5j	Br	2-OCH ₃	1.32 ± 0.52
5k	Br	5-Br	0.82 ± 0.36
5l	Br	6-Br	0.86 ± 0.67
5m	Br	6-Cl	0.77 ± 0.64
5n	Br	6-OCH ₃	1.15 ± 0.31
5o	CH ₃	2-F	0.78 ± 0.44
5p	CH ₃	2-Cl	0.84 ± 0.24
5q	CH ₃	2-OCH ₃	1.88 ± 0.87
5r	CH ₃	5-Br	0.95 ± 0.71
5s	CH ₃	6-Br	1.02 ± 0.33
5t	CH ₃	6-Cl	0.85 ± 0.61
5u	CH ₃	6-OCH ₃	1.79 ± 0.94
Vemurafenib ^a			0.03 ± 0.005

^a Used as a positive control.

Structure activity relationships of 5-phenyl-1H-pyrazole derivatives demonstrated that compounds with *para* electron-donating substituents on phenyl ring A showed more potent inhibitory activities than those with electron-withdrawing substituents and the potency order is Me > H > Br. In the case of constant A ring substituents, change of substituents on B-ring could also affect the activities of compounds and the inhibitory activities of compounds with different substituents on ring B increased in the following order: 2-OMe < 6-OMe < 6-Br < 5-Br < 6-Cl < 2-Cl < 2-F. This result indicated that the strong electronic-withdrawing substituents on phenyl ring B were beneficial for the activity. Among all the compounds, **5h** with *p*-Me group on the A-ring and 2-F group on the B-ring showed the best activity.

The results of BRAF^{V600E} kinases inhibitory activities of the test compounds were corresponding to the structure activity relationships (SAR) of their antitumor activities. It demonstrated that the potent antitumor activities of the synthesized compounds were probably correlated to their BRAF^{V600E} kinases inhibitory activities.

2.3. Molecular docking

To gain better understanding of the structure–activity relationships observed, molecular docking of the most potent inhibitor **5h** into the active site cavity of BRAF^{V600E} kinases was performed on the binding model based on the BRAF^{V600E} crystal structure (PDB code: 2FB8). The molecular docking was performed by inserting compound **5h** into the SB-590885 binding site of BRAF^{V600E}. All docking runs were applied LigandFit Dock protocol of Discovery Studio 3.5. The binding modes of compound **5h** and BRAF^{V600E} were depicted in Figure 1, and the enzyme surface model was shown in Figure 2, which revealed that the molecule is well filled in the active pocket. The amino acid residues which had interaction with BRAF^{V600E} were labeled.

In the binding mode, compound **5h** is nicely bound to BRAF^{V600E} via one hydrogen bond and three π–π interactions. As illustrated in Figure 1, one fluorine atom on the nicotinamide ring and the hydrogen atom on the main chain of Thr529 (angle N–H...F = 129.2°, distance = 2.41 Å) contribute to the hydrogen bonding interaction together, being a probable explanation for its nice activity. One π–π interaction is formed between the benzene rings of the compound **5h** and Trp531. Two π–π interactions are formed between the pyrazolyl ring of the compound **5h** and Trp531 and Phe583 respectively. Meanwhile, the receptor surface model showed in Figure 2 revealed that this candidate BRAF^{V600E} inhibitor was tightly embedded into the ATP binding pocket. This molecular docking result, along with the biological assay data, suggested that compound **5h** is a potential inhibitor of BRAF^{V600E}.

2.3.1. 3D-QSAR

In order to acquire a systematic SAR profile on the synthesized compounds and to explore the more powerful and selective BRAF^{V600E} inhibitors, 3D-QSAR model was built to choose activity conformation of the designed molecular and reasonably evaluated the designed molecules by using the corresponding pIC₅₀ values which were converted from the obtained IC₅₀ (μM) values of BRAF^{V600E} inhibition and performed by built-in QSAR software of DS 3.5 (Discovery Studio 3.5, Accelrys, Co. Ltd). By convention, the pIC₅₀ scale (–logIC₅₀), in which higher values indicate exponentially greater potency, is used as a method to measure inhibitory activity. The training and test set was chosen by the Diverse Molecules method in Discovery Studio. Considering a good alignment is very important for the analysis of molecular fields, we applied CDOCKER protocol to explore each molecule with lowest energy before alignment conformation. 5-Phenyl-1H-pyrazole was selected as substructure to build alignment conformation before building the QSAR model.

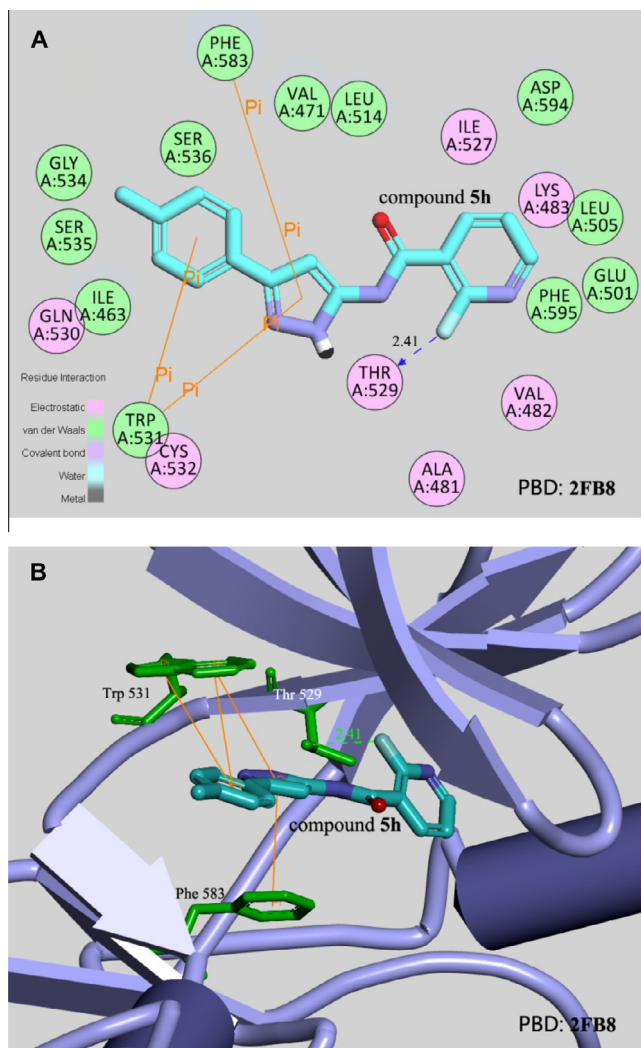


Figure 1. Binding mode of compound **5h** with BRAF^{V600E} kinase. For clarity, only interacting residues were labeled. Hydrogen bonding interactions are shown in green dotted lines. This figure was made using PyMol.

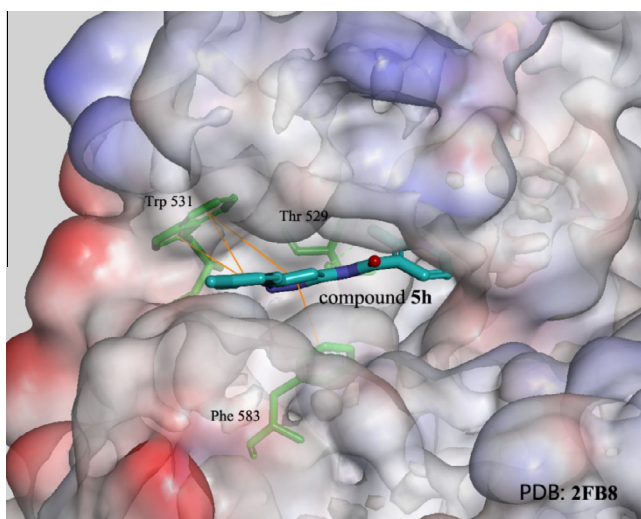


Figure 2. Binding mode of compound **5h** with BRAF^{V600E} kinase. The enzyme is shown as surface; while **5h** docked structures are shown as sticks. This figure was made using PyMol.

Table 3

Experimental, predicted inhibitory activity of compounds **5a–5u** by 3D-QSAR models based upon active conformation achieved by molecular docking

Compound ^a	BRAFF ^{V600E}		Residual error
	Actual pIC ₅₀	Predicted pIC ₅₀	
5a	6.252	6.157	0.095
5b	6.125	6.158	-0.033
5c	5.812	5.863	-0.051
5d	6.009	6.026	-0.017
5e	5.917	5.956	-0.039
5f	6.076	5.977	0.099
5g	5.824	5.783	0.041
5h	6.481	6.463	0.018
5i	6.161	6.176	-0.015
5j	5.879	5.900	-0.021
5k	6.086	6.146	-0.060
5l	6.066	6.002	0.064
5m	6.114	6.105	0.009
5n	5.939	5.939	0.000
5o	6.108	6.102	0.006
5p	6.076	6.086	-0.010
5q	5.726	5.795	-0.069
5r	6.022	6.121	-0.099
5s	5.991	5.981	0.010
5t	6.071	5.928	0.143
5u	5.747	5.757	-0.010

^a Underlined compounds were selected as the test sets while the rest ones were in the training sets.

The correlation coefficient r^2 between observed and predicted activity of training set was found to be 0.879, while that of test set was found to be 0.973, which proved that the QSAR model built by us was acceptable. Predicted pIC₅₀ values and residual errors of 21 compounds by this QSAR model had been given in Table 3. The well agreement between predicted pIC₅₀ value and experimental pIC₅₀ value for both test sets and training sets are shown in Figure 3.

Also the molecules aligned with the iso-surfaces of the 3D-QSAR model coefficients on electrostatic potential grids (Fig. 4a) and van der Waals grids (Fig. 4b) are listed. Electrostatic map indicates red contours around regions where high electron density (negative charge) is expected to increase activity, and blue contours represent areas where low electron density (partial positive charge) is expected to increase activity. Similarly, steric map indicates areas

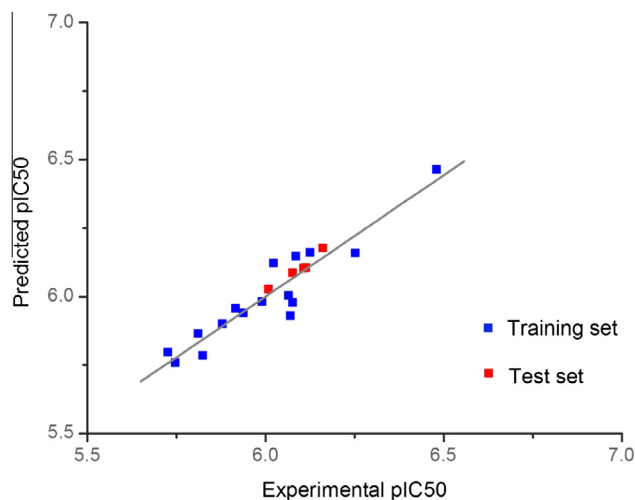


Figure 3. Plot of experimental versus predicted BRAF^{V600E} inhibitory activities of training set and test set.

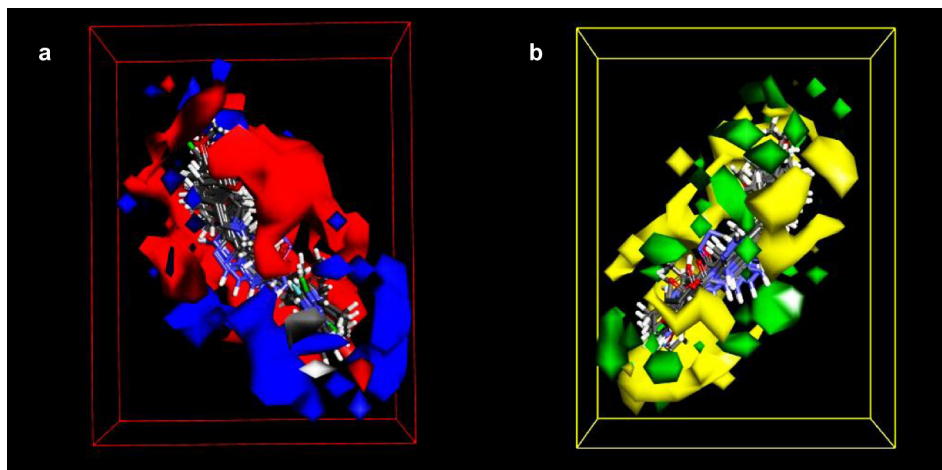


Figure 4. (a) 3D-QSAR model coefficients on electrostatic potential grids. Blue represents positive coefficients; red represents negative coefficients. (b) 3D-QSAR model coefficients on van der Waals grids. Green represents positive coefficients; yellow represents negative coefficients.

where steric bulk is predicted to increase (green) or decrease (yellow) activity.

According to the maps, it suggested that the compound with high negative charged and small R_2 group, would show higher activity, validating that halogen substituted group being a better choice than methoxy substituted group and F substituent better than Cl as well as Cl substituent better than Br. Whereas, a low negative charged and bulky R_1 group would help obtain sound activity, validating the 4-Me substituent could be more effective. As a result, data summarized above demonstrated that compounds **5h**, the most potent BRAF^{V600E} inhibitor ($IC_{50} = 0.33 \mu\text{M}$), containing suitable substituents had an outstanding activity. Thus, this promising model would provide a guideline to design and optimize more effective BRAF^{V600E} inhibitors and pave the way for us in the further study.

3. Conclusion

In this study, a series of novel BRAF inhibitors beared pyrazole core and niacinamide moiety have been synthesized and evaluated their biological activities. Most of these compounds displayed good inhibitory BRAF^{V600E} activities and potent antiproliferative activity against WM266.4 cell lines and A375 cell lines. Among them, compound **5h** exhibited the most potent BRAF^{V600E} inhibition activities ($IC_{50} = 0.33 \mu\text{M}$ for BRAF^{V600E}) and antiproliferative activities ($IC_{50} = 2.63 \mu\text{M}$ for WM266.4 and $IC_{50} = 3.16 \mu\text{M}$ for A375). Docking simulation was performed to put compound **5h** into the BRAF^{V600E} protein active site to determine the potential binding model and found that several interactions with the protein residues in the BRAF^{V600E} protein active site might play an important role in its antiproliferative activities. QSAR model was built to provide a reliable tool for reasonable design of novel BRAF^{V600E} inhibitors in future.

4. Experiments

4.1. Materials and measurements

All chemicals and reagents used in current study were analytical grade. TLC was performed on the glass-backed silica gel sheets (Silica Gel 60 GF254) and visualized in UV light (254 nm). Column chromatography was performed using silica gel (200–300 mesh) eluting with ethyl acetate and petroleum ether. The quantity of

silica gel used was 50–100 times the weight charged on the column. Melting points (uncorrected) were determined on a XT4MP apparatus (Taike Corp., Beijing, China). All the Proton nuclear magnetic resonance (¹H NMR) spectra were recorded on a Bruker PX400 or DPX300 model Spectrometer in DMSO-*d*₆ at 25 °C with TMS and chemical shifts were reported in parts per million (δ). The solvent signals allotted as internal stands. Elemental analyses were performed on a CHN-O-Rapid instrument. All the compounds gave satisfactory chemical analyses (±0.4%).

4.2. General procedure for the synthesis of 2a–2c

Mixed *p*-substituted methyl benzoate (7 mmol) with NaH (14 mmol, 0.35 g) in boiling tetrahydrofuran (5 mL) and then followed by dropwise addition of solution of acetonitrile (7 mmol, 0.29 g, 0.4 mL) in tetrahydrofuran (1 mL). The resulting mixture was refluxed for 4 h and then cooling down to room temperature, after which the solution was diluted with diethylether (15 mL) and left to stand at room temperature for 48 h. The precipitated sodium salt was filtered and washed with diethylether. The dry compound was dissolved in water (5 mL) and acidified with HCl (1 mol/L) to pH 2. The collected extracts were crystallized from toluene, filtered and dried with Na₂SO₄.

4.3. General procedure for the synthesis of 3a–3c

To a stirred mixture of compound **2a–2c** (5 mmol) in EtOH (25 mL) were added NH₂NH₂·H₂O (0.3 mL, 6 mmol) and CH₃SO₃H (0.1 mL, 1 mmol) at room temperature and the mixture was stirred under reflux for 1 h. The precipitate was purified by column chromatography over silica gel to give the compound **3a–3c**.

4.4. General procedure for the synthesis of 5-phenyl-1H-pyrazole derivatives (5a–5u)

Compounds **5a–5w** were synthesized by coupling substituted **3a–3c** with nicotinic acids, using 1-ethyl-3-(3-dimethylaminopropyl)carbodiimide hydrochloride (EDCI) and *N*-hydroxybenzotriazole (HOBT) as condensing agent. The mixture was refluxed in anhydrous CH₂Cl₂ for 1–3 h. The products were extracted with ethyl acetate. The extract was washed successively with 5% HCl, then evaporated and purified by column chromatography over silica gel to give the compound.

4.4.1. 2-Fluoro-N-(5-phenyl-1H-pyrazol-3-yl)nicotinamide (5a)

Yellow powder, yield: 76%. Mp 176–177 °C. ¹H NMR (300 MHz, DMSO, δ ppm): 5.90 (s, 1H); 6.93 (s, 2H); 7.38–7.40 (m, 3H); 7.55–7.59 (m, 1H); 7.65–7.67 (m, 2H); 8.35–8.39 (m, 1H); 8.48 (d, $J = 3.0$ Hz, 1H). MS (ESI): 283.45 [M+H]⁺. Anal. Calcd for C₁₅H₁₁FN₄O: C, 63.83; H, 3.93; N, 19.85; Found: C, 68.71; H, 3.78; N, 19.62.

4.4.2. 2-Chloro-N-(5-phenyl-1H-pyrazol-3-yl)nicotinamide (5b)

Yellow powder, yield: 82%. Mp 134–135 °C. ¹H NMR (300 MHz, DMSO, δ ppm): 5.87 (s, 1H); 6.91 (s, 2H); 7.36–7.38 (m, 3H); 7.59–7.63 (m, 3H); 8.21 (dd, $J_1 = 1.8$ Hz, $J_2 = 7.5$ Hz, 1H); 8.59 (dd, $J_1 = 1.8$ Hz, $J_2 = 4.8$ Hz, 1H). MS (ESI): 299.67 [M+H]⁺. Anal. Calcd for C₁₅H₁₁ClN₄O: C, 60.31; H, 3.71; N, 18.76; Found: C, 60.21; H, 3.68; N, 18.82.

4.4.3. 2-Methoxy-N-(5-phenyl-1H-pyrazol-3-yl)nicotinamide (5c)

Yellow powder, yield: 68%. Mp 187–188 °C. ¹H NMR (300 MHz, DMSO, δ ppm): 3.87 (s, 3H); 5.85 (s, 1H); 6.85 (s, 2H); 7.14–7.17 (m, 1H); 7.37 (d, $J = 4.8$ Hz, 3H); 7.61–7.63 (m, 2H); 7.96–7.98 (m, 1H); 8.36 (dd, $J_1 = 1.4$ Hz, $J_2 = 3.8$ Hz, 1H). MS (ESI): 295.44 [M+H]⁺. Anal. Calcd for C₁₆H₁₄N₄O₂: C, 65.30; H, 4.79; N, 19.04; Found: C, 65.21; H, 4.68; N, 18.92.

4.4.4. 5-Bromo-N-(5-phenyl-1H-pyrazol-3-yl)nicotinamide (5d)

Yellow powder, yield: 64%. Mp 130–131 °C. ¹H NMR (300 MHz, DMSO, δ ppm): 5.92 (s, 1H); 6.92 (s, 2H); 7.43 (d, $J = 7.2$ Hz, 3H); 7.73–7.76 (m, 2H); 8.65 (s, 1H); 8.95 (d, $J = 2.2$ Hz, 1H); 9.15 (d, $J = 1.5$ Hz, 1H). MS (ESI): 344.26 [M+H]⁺. Anal. Calcd for C₁₅H₁₁BrN₄O: C, 52.50; H, 3.23; N, 16.33; Found: C, 52.40; H, 3.33; N, 16.51.

4.4.5. 6-Bromo-N-(5-phenyl-1H-pyrazol-3-yl)nicotinamide (5e)

Yellow powder, yield: 75%. Mp 156–157 °C. ¹H NMR (300 MHz, DMSO, δ ppm): 5.92 (s, 1H); 6.93 (s, 2H); 7.43 (d, $J = 5.8$ Hz, 3H); 7.76–7.78 (m, 2H); 7.89 (d, $J = 6.2$ Hz, 1H); 8.36–8.37 (m, 1H); 9.02 (d, $J = 1.5$ Hz, 1H). MS (ESI): 344.68 [M+H]⁺. Anal. Calcd for C₁₅H₁₁BrN₄O: C, 52.50; H, 3.23; N, 16.33; Found: C, 52.71; H, 3.48; N, 16.42.

4.4.6. 2-Chloro-N-(5-phenyl-1H-pyrazol-3-yl)nicotinamide (5f)

Yellow powder, yield: 83%. Mp 259–261 °C. ¹H NMR (300 MHz, DMSO, δ ppm): 7.04 (s, 1H); 7.36 (d, $J = 4.2$ Hz, 1H); 7.44 (t, $J = 9.0$ Hz, 2H); 7.67 (d, $J = 4.9$ Hz, 1H); 7.75 (d, $J = 4.6$ Hz, 2H); 8.38 (m, 1H); 8.98 (d, $J = 1.3$ Hz, 1H); 11.17 (s, 1H); 13.00 (s, 1H). ¹³C NMR (300 MHz, DMSO-*d*₆) δ : 167.2, 155.7, 152.9, 151.4, 146.6, 139.2, 139.0, 131.8, 129.7, 129.7, 129.4, 126.4, 126.4, 123.2, 85.5, 21.4. MS (ESI): 299.84 [M+H]⁺. Anal. Calcd for C₁₅H₁₁ClN₄O: C, 60.31; H, 3.71; N, 18.76; Found: C, 60.19; H, 3.13; N, 18.32.

4.4.7. 6-Methoxy-N-(5-phenyl-1H-pyrazol-3-yl)nicotinamide (5g)

Yellow powder, yield: 66%. Mp 102–103 °C. ¹H NMR (300 MHz, DMSO, δ ppm): 3.93 (s, 3H); 5.91 (s, 1H); 6.87 (s, 2H); 7.00 (d, $J = 6.4$ Hz, 1H); 7.46 (d, $J = 5.4$ Hz, 2H); 7.76–7.80 (m, 3H); 8.45 (dd, $J_1 = 1.8$ Hz, $J_2 = 6.6$ Hz, 1H); 9.04 (d, $J = 1.6$ Hz, 1H). MS (ESI): 295.42 [M+H]⁺. Anal. Calcd for C₁₆H₁₄N₄O₂: C, 65.30; H, 4.79; N, 19.04; Found: C, 65.21; H, 4.68; N, 18.82.

4.4.8. 2-Fluoro-N-(5-(*p*-tolyl)-1H-pyrazol-3-yl)nicotinamide (5h)

Yellow powder, yield: 58%. Mp 146–147 °C. ¹H NMR (300 MHz, DMSO, δ ppm): 2.30 (s, 3H); 5.86 (s, 1H); 6.90 (s, 2H); 7.20 (d, $J = 6.0$ Hz, 2H); 7.55 (d, $J = 6.1$ Hz, 3H); 8.33–8.38 (m, 1H); 8.47 (d, $J = 2.5$ Hz, 1H). MS (ESI): 297.45 [M+H]⁺. Anal. Calcd for C₁₆H₁₃

FN₄O: C, 64.86; H, 4.42; N, 18.91; Found: C, 64.71; H, 4.48; N, 18.81.

4.4.9. 2-Chloro-N-(5-(*p*-tolyl)-1H-pyrazol-3-yl)nicotinamide (5i)

Yellow powder, yield: 60%. Mp 146–147 °C. ¹H NMR (300 MHz, DMSO, δ ppm): 2.29 (s, 3H); 5.84 (s, 1H); 6.89 (s, 2H); 7.18 (d, $J = 7.9$ Hz, 2H); 7.50 (d, $J = 8.1$ Hz, 2H); 7.61 (dd, $J_1 = 4.9$ Hz, $J_2 = 7.5$ Hz, 1H); 8.20 (dd, $J_1 = 1.7$ Hz, $J_2 = 7.5$ Hz, 1H); 8.59 (dd, $J_1 = 1.7$ Hz, $J_2 = 4.7$ Hz, 1H). MS (ESI): 314.62 [M+H]⁺. Anal. Calcd for C₁₆H₁₃ClN₄O: C, 61.44; H, 4.19; N, 17.91; Found: C, 61.39; H, 4.22; N, 17.87.

4.4.10. 2-Methoxy-N-(5-(*p*-tolyl)-1H-pyrazol-3-yl)nicotinamide (5j)

Yellow powder, yield: 58%. Mp 145–146 °C. ¹H NMR (300 MHz, DMSO, δ ppm): 2.30 (s, 3H); 5.81 (s, 1H); 6.82 (s, 2H); 7.07 (s, 1H); 7.40–7.43 (m, 5H); 8.16–8.18 (m, 2H). MS (ESI): 309.23 [M+H]⁺. Anal. Calcd for C₁₇H₁₆N₄O₂: C, 66.22; H, 5.23; N, 18.17; Found: C, 66.01; H, 5.48; N, 18.32.

4.4.11. 5-Bromo-N-(5-(*p*-tolyl)-1H-pyrazol-3-yl)nicotinamide (5k)

Yellow powder, yield: 78%. Mp 191–192 °C. ¹H NMR (300 MHz, DMSO, δ ppm): 5.88 (s, 1H); 6.90 (s, 2H); 7.24 (d, $J = 8.0$ Hz, 2H); 7.63 (d, $J = 8.0$ Hz, 2H); 8.64 (s, 1H); 8.94 (s, 1H); 9.14 (s, 1H). MS (ESI): 358.43 [M+H]⁺. Anal. Calcd for C₁₆H₁₃BrN₄O: C, 53.80; H, 3.67; N, 15.68; Found: C, 53.77; H, 3.68; N, 15.56.

4.4.12. 6-Bromo-N-(5-(*p*-tolyl)-1H-pyrazol-3-yl)nicotinamide (5l)

Yellow powder, yield: 64%. Mp 178–179 °C. ¹H NMR (300 MHz, DMSO, δ ppm): 2.34 (s, 3H); 5.88 (s, 1H); 6.91 (s, 2H); 7.24 (d, $J = 6.1$ Hz, 2H); 7.66 (d, $J = 6.1$ Hz, 2H); 7.88 (d, $J = 6.3$ Hz, 1H); 8.36–8.38 (m, 1H); 9.03 (d, $J = 1.8$ Hz, 1H). MS (ESI): 358.61 [M+H]⁺. Anal. Calcd for C₁₆H₁₃BrN₄O: C, 53.80; H, 3.67; N, 15.68; Found: C, 53.71; H, 3.58; N, 15.82.

4.4.13. 6-Chloro-N-(5-(*p*-tolyl)-1H-pyrazol-3-yl)nicotinamide (5m)

Yellow powder, yield: 67%. Mp 152–153 °C. ¹H NMR (300 MHz, DMSO, δ ppm): 2.33 (s, 3H); 5.88 (s, 1H); 6.89 (s, 2H); 7.24 (d, $J = 7.9$ Hz, 2H); 7.66 (d, $J = 8.0$ Hz, 2H); 7.34 (d, $J = 8.4$ Hz, 1H); 8.49 (dd, $J_1 = 2.2$ Hz, $J_2 = 8.2$ Hz, 1H); 9.06 (d, $J = 2.0$ Hz, 1H). ¹³C NMR (300 MHz, DMSO-*d*₆) δ : 167.1, 155.2, 153.5, 152.2, 142.4, 139.3, 129.7, 129.7, 129.5, 129.3, 128.7, 126.4, 126.4, 124.1, 85.3, 21.4. MS (ESI): 314.52 [M+H]⁺. Anal. Calcd for C₁₆H₁₃ClN₄O: C, 61.44; H, 4.19; N, 17.91; Found: C, 61.40; H, 4.08; N, 17.88.

4.4.14. 6-Methoxy-N-(5-(*p*-tolyl)-1H-pyrazol-3-yl)nicotinamide (5n)

Yellow powder, yield: 59%. Mp 125–126 °C. ¹H NMR (300 MHz, DMSO, δ ppm): 2.33 (s, 3H); 3.98 (s, 3H); 5.87 (s, 1H); 6.84 (s, 2H); 6.99 (d, $J = 8.8$ Hz, 1H); 7.24 (d, $J = 8.0$ Hz, 2H); 7.68 (d, $J = 8.0$ Hz, 2H); 8.73 (s, 1H); 9.03 (d, $J = 2.4$ Hz, 1H). MS (ESI): 309.44 [M+H]⁺. Anal. Calcd for C₁₇H₁₆N₄O₂: C, 66.22; H, 5.23; N, 18.17; Found: C, 66.02; H, 5.03; N, 18.25.

4.4.15. N-(5-(4-Bromophenyl)-1H-pyrazol-3-yl)-2-fluoronicotinamide (5o)

Yellow powder, yield: 66%. Mp 146–147 °C. ¹H NMR (300 MHz, DMSO, δ ppm): 5.91 (s, 1H); 6.96 (s, 2H); 7.61 (s, 4H); 7.70–7.76 (m, 1H); 8.34–8.38 (m, 1H); 8.48 (d, $J = 3.2$ Hz, 1H). ¹³C NMR (300 MHz, DMSO-*d*₆) δ : 165.8, 154.4, 153.1, 150.5, 142.4, 132.6, 132.1, 132.1, 131.4, 128.4, 128.4, 128.3, 123.0, 122.3, 118.3, 85.5. MS (ESI): 362.37 [M+H]⁺. Anal. Calcd for C₁₅H₁₀BrFN₄O: C, 49.88; H, 2.79; N, 15.51; Found: C, 50.01; H, 2.68; N, 15.62.

4.4.16. N-(5-(4-Bromophenyl)-1H-pyrazol-3-yl)-2-chloronicotinamide (5p)

Yellow powder, yield: 85%. Mp 171–172 °C. ¹H NMR (300 MHz, DMSO, δ ppm): 5.90 (s, 1H); 6.98 (s, 2H); 7.58 (s, 4H); 7.60–7.63 (m, 1H); 8.22 (dd, $J_1 = 1.4$ Hz, $J_2 = 5.7$ Hz, 1H); 8.60 (dd, $J_1 = 1.4$ Hz, $J_2 = 3.6$ Hz, 1H). MS (ESI): 377.62 [M+H]⁺. Anal. Calcd for C₁₅H₁₀BrClN₄O: C, 47.71; H, 2.67; N, 14.84; Found: C, 47.59; H, 2.58; N, 14.62.

4.4.17. N-(5-(4-Bromophenyl)-1H-pyrazol-3-yl)-2-methoxynicotinamide (5q)

Yellow powder, yield: 73%. Mp 207–208 °C. ¹H NMR (300 MHz, DMSO, δ ppm): 3.86 (s, 3H); 5.86 (s, 1H); 6.88 (s, 2H); 7.13–7.16 (m, 1H); 7.57 (s, 4H); 7.95–7.98 (m, 1H); 8.35–8.37 (m, 1H). MS (ESI): 374.46 [M+H]⁺. Anal. Calcd for C₁₆H₁₃BrN₄O₂: C, 51.49; H, 3.51; N, 15.01; Found: C, 51.31; H, 3.68; N, 14.82.

4.4.18. 5-Bromo-N-(5-(4-bromophenyl)-1H-pyrazol-3-yl)nicotinamide (5r)

Yellow powder, yield: 59%. Mp 227–228 °C. ¹H NMR (300 MHz, DMSO, δ ppm): 5.93 (s, 1H); 7.65–7.71 (m, 6H); 8.61 (s, 1H); 8.94 (s, 1H); 9.14 (s, 1H). MS (ESI): 423.19 [M+H]⁺. Anal. Calcd for C₁₅H₁₀Br₂N₄O: C, 42.68; H, 2.39; N, 13.27; Found: C, 42.33; H, 2.45; N, 13.22.

4.4.19. 6-Bromo-N-(5-(4-bromophenyl)-1H-pyrazol-3-yl)nicotinamide (5s)

Yellow powder, yield: 86%. Mp 205–206 °C. ¹H NMR (300 MHz, DMSO, δ ppm): 5.91 (s, 1H); 7.72–7.83 (m, 6H); 8.59 (s, 1H); 8.88 (s, 1H); 9.12 (s, 1H). MS (ESI): 422.38 [M+H]⁺. Anal. Calcd for C₁₅H₁₀Br₂N₄O: C, 42.68; H, 2.39; N, 13.27; Found: C, 42.51; H, 2.16; N, 13.75.

4.4.20. N-(5-(4-Bromophenyl)-1H-pyrazol-3-yl)-6-chloronicotinamide (5t)

Yellow powder, yield: 58%. Mp 178–179 °C. ¹H NMR (300 MHz, DMSO, δ ppm): 5.93 (s, 1H); 6.95 (s, 2H); 7.63 (d, $J = 8.6$ Hz, 2H); 7.71–7.75 (m, 3H); 8.46–8.50 (m, 1H); 9.05 (d, $J = 2.2$ Hz, 1H). MS (ESI): 378.77 [M+H]⁺. Anal. Calcd for C₁₅H₁₀BrClN₄O: C, 47.71; H, 2.67; N, 14.84; Found: C, 47.66; H, 2.75; N, 14.94.

4.4.21. N-(5-(4-Bromophenyl)-1H-pyrazol-3-yl)-6-methoxynicotinamide (5u)

Yellow powder, yield: 78%. Mp 217–218 °C. ¹H NMR (300 MHz, DMSO, δ ppm): 2.41 (s, 3H); 5.92 (s, 1H); 6.89 (s, 2H); 6.99 (d, $J = 8.8$ Hz, 1H); 7.64 (d, $J = 8.6$ Hz, 2H); 7.75 (d, $J = 8.5$ Hz, 2H); 8.40–8.44 (m, 1H); 9.02 (d, $J = 2.1$ Hz, 1H). MS (ESI): 374.35 [M+H]⁺. Anal. Calcd for C₁₆H₁₃BrN₄O₂: C, 51.49; H, 3.51; N, 15.01; Found: C, 51.38; H, 3.64; N, 14.94.

4.5. Antiproliferation activity

WM1361, WM266.4 and A375 cell lines were cultured in DMEM/10% fetal bovine serum, in 5% CO₂ water saturated atmosphere at 37 °C. Cell suspensions (10,000/mL) were prepared and 100 mL/well dispensed into 96-well plates (Costar) giving 1000 cells/well. The plates were returned to the incubator for 24 h to allow the cells to reattach. Tested samples at pre-set concentrations were added to six wells with vemurafenib as positive references. After 48 h exposure period, 40 μ L of PBS containing 2.5 mg/mL of MTT (3-(4,5-dimethylthiazol-2-yl)-2,5-diphenyltetrazolium bromide) was added to each well. Four hours later, 100 μ L extraction solution (10% SDS–5% isobutyl alcohol–0.01 M HCl) was added. After an overnight incubation at 37 °C, the optical density was measured at a wavelength of 570 nm on an ELISA microplate reader. In all experiments three replicate wells were

used for each drug concentration. Each assay was carried out for at least three times.

4.6. Kinase assay

The BRAF Kinase inhibitory activity was measured using previously methods described by J. Dietrich et al.³² The assay was performed in triplicate for each tested compound in this study. Briefly, 7.5 ng Mouse Full-Length GST-tagged BRAF^{V600E} (Invitrogen, PV3849) was pre-incubated at room temperature for 1 h with 1 μ L drug and 4 μ L assay dilution buffer. The kinase assay was initiated when 5 μ L of a solution containing 200 ng recombinant human full length, N-terminal His-tagged MEK1 (Invitrogen), 200 μ M ATP (0.8 μ Ci hot ATP), and 30 mM MgCl₂ in assay dilution buffer was added. The kinase reaction was allowed to continue at room temperature for 25 min and was then quenched with 5 μ L 5 \times protein denaturing buffer (LDS) solution. Protein was further denatured by heating for 5 min at 70 °C. 10 μ L of 20 each reaction was loaded into a 15-well, 4–12% precast NuPage gel (Invitrogen) and run at 200 V, and upon completion, the front, which contained excess hot ATP, was cut from the gel and discarded. The gel was then dried and developed onto a phosphor screen. A reaction that contained no active enzyme was used as a negative control, and a reaction without inhibitor was used as the positive control.

4.7. Docking simulations

The crystal structures of BRAF^{V600E} (PDB code: 2FB8) was obtained from the Protein Data Bank (<http://www.rcsb.org>). Molecular docking of compound **5h** into the three-dimensional X-ray structure of BRAF^{V600E} was carried out using CDOCKER Dock protocol of Discovery Studio 3.5. All bound water and ligands were eliminated from the protein and the polar hydrogen was added. The whole BRAF^{V600E} complex was defined as a receptor and the site sphere was selected based on the ligand binding location of SB-590885, then the SB-590885 molecule was removed and **5h** was placed during the molecular docking procedure.

4.8. QSAR model

Among all the 21 compounds, 81% (that is 17) were utilized as a training set for QSAR modeling and the remaining 19% (that is 4) were chosen as an external test subset for validating the reliability of the QSAR model by the Diverse Molecules protocol in Discovery Studio 3.5. The selected test compounds were: **5d**, **5i**, **5o**, **5p**.

The inhibitory activity of the compounds in literatures [IC₅₀ (mol/L)] was initially changed into the minus logarithmic scale [IC₅₀ (mol/L)] and then used for subsequent QSAR analysis as the response variable.

In Discovery Studio, the CHARMM force field is used and the electrostatic potential and the van der Waals potential are treated as separate terms. A+1e point charge is used as the electrostatic potential probe and distance-dependent dielectric constant is used to mimic the solvation effect. For the van der Waals potential a carbon atom with a 1.73 Å radius is used as a probe.

A Partial Least-Squares (PLS) model is built using energy grids as descriptors. QSAR models were built by using the Create 3D QSAR Model protocol in Discovery Studio 3.5.

Acknowledgements

This work was supported by Natural Science Foundation of Jiangsu Province (No. BK20130554) and supported by Major Projects on Control and Rectification of Water Body Pollution (No. 2011ZX07204-001-2214 004).

References and notes

- Halilovic, E.; Solit, D. B. *Curr. Opin. Pharmacol.* **2008**, *8*, 419.
- McCubrey, J. A.; Milella, M.; Tafuri, A.; Martelli, A. M.; Lunghi, P.; Bonati, A.; Cervello, M.; Lee, J. T.; Steelman, L. S. *Curr. Opin. Invest. Drugs* **2008**, *9*, 614.
- Michaloglou, C.; Vredeveld, L. C.; Mooi, W. J.; Peeper, D. S. *Oncogene* **2008**, *27*, 877.
- Beck, T. W.; Huleihel, M.; Gunnell, M.; Bonner, T. I.; Rapp, U. R. *Nucleic Acids Res.* **1987**, *15*, 595.
- Bonner, T. I.; Kerby, S. B.; Suttrave, P.; Gunnell, M. A.; Mark, G.; Rapp, U. R. *Mol. Cell. Biol.* **1985**, *5*, 1400.
- Huebner, K.; ar-Rushdi, A.; Griffin, C. A.; Isobe, M.; Kozak, C.; Emanuel, B. S.; Nagarajan, L.; Cleveland, J. L.; Bonner, T. I.; Goldsborough, M. D. *Proc. Natl. Acad. Sci. U.S.A.* **1986**, *83*, 3934.
- Ikawa, S.; Fukui, M.; Ueyama, Y.; Tamaoki, N.; Yamamoto, T.; Toyoshima, K. *Mol. Cell. Biol.* **1988**, *8*, 2651.
- Wellbrock, C.; Karasarides, M.; Marais, R. *Nat. Rev. Mol. Cell. Biol.* **2004**, *5*, 875.
- Guan, K. L.; Figueroa, C.; Brtva, T. R.; Zhu, T.; Taylor, J.; Barber, T. D.; Vojtek, A. B. *Biol. Chem.* **2000**, *275*, 27354.
- Gray-Schopfer, V.; Wellbrock, C.; Marais, R. *Nature* **2007**, *445*, 851.
- Davies, H.; Bignell, G. R.; Cox, C.; Stephens, P.; Edkins, S.; Clegg, S.; Teague, J.; Woffendin, H.; Garnett, M. J.; Bottomley, W.; Davis, N.; Dicks, E.; Ewing, R.; Floyd, Y.; Gray, K.; Hall, S.; Hawes, R.; Hughes, J.; Kosmidou, V.; Menzies, A.; Mould, C.; Parker, A.; Stevens, C.; Watt, S.; Hooper, S.; Wilson, R.; Jayatilake, H.; Gusterson, B. A.; Cooper, C.; Shipley, J.; Hargrave, D.; Pritchard-Jones, K.; Maitland, N.; Chenevix-Trench, G.; Riggins, G. J.; Bigner, D. D.; Palmieri, G.; Cossu, A.; Flanagan, A.; Nicholson, A.; Ho, J. W.; Leung, S. Y.; Yuen, S. T.; Weber, B. L.; Seigler, H. F.; Darrow, T. L.; Paterson, H.; Marais, R.; Marshall, C. J.; Wooster, R.; Stratton, M. R.; Futreal, P. A. *Nature* **2002**, *417*, 949.
- McCubrey, J. A.; Milella, M.; Tafuri, A.; Martelli, A. M.; Lunghi, P.; Bonati, A.; Cervello, M.; Lee, J. T.; Steelman, L. S. *Curr. Opin. Invest. Drugs* **2008**, *9*, 614.
- King, A. J.; Patrick, D. R.; Batorsky, R. S.; Ho, M. L.; Do, H. T.; Zhang, S. Y.; Kumar, R.; Rusnak, D. W.; Takle, A. K.; Wilson, D. M.; Hugger, E.; Wang, L.; Karreth, F.; Lougheed, J. C.; Lee, J.; Chau, D.; Stout, T. J.; May, E. W.; Rominger, C. M.; Schaber, M. D.; Luo, L.; Lakdawala, A. S.; Adams, J. L.; Contractor, R. G.; Smalley, K. S. M.; Herlyn, M.; Morrissey, M. M.; Tuveson, D. A.; Huang, P. S. *Cancer Res.* **2006**, *66*, 11100.
- McDermott, U.; Sharma, S. V.; Dowell, L.; Greninger, P.; Montagut, C.; Lamb, J.; Archibald, H.; Raudales, R.; Tam, A.; Lee, D.; Rothenberg, S. M.; Supko, J. G.; Sordella, R.; Ulkus, L. E.; Iafrate, A. J.; Maheswaran, S.; Njauw, C. N.; Tsao, H.; Drew, L.; Hanke, J. H.; Ma, X.-J.; Erlander, M. G.; Gray, N. S.; Haber, D. A.; Settleman, J. *Proc. Natl. Acad. Sci. U.S.A.* **2007**, *104*, 19936.
- Roberts, P. J.; Der, C. J. *Oncogene* **2007**, *26*, 3291.
- Flaherty, K. T.; Puzanov, I.; Kim, K. B.; Ribas, A.; McArthur, G. A.; Sosman, J. A.; O'Dwyer, P. J.; Lee, R. J.; Grippo, J. F.; Nolop, K.; Chapman, P. B. *N. Engl. J. Med.* **2010**, *363*, 809.
- Bollag, G.; Hirth, P.; Tsai, J.; Zhang, J.; Ibrahim, P. N.; Cho, H.; Spevak, W.; Zhang, C.; Zhang, Y.; Habets, G.; Burton, E. A.; Wong, B.; Tsang, G.; West, B. L.; Powell, B.; Shellooe, R.; Marimuthu, A.; Nguyen, H.; Zhang, K. Y. J.; Artis, D. R.; Schlessinger, J.; Su, F.; Higgins, B.; Iyer, R.; Dndrea, K.; Koehler, A.; Stumm, M.; Lin, P. S.; Lee, R. J.; Grippo, J.; Puzanov, I.; Kim, K. B.; Ribas, A.; McArthur, G. A.; Sosman, J. A.; Chapman, P. B.; Flaherty, K. T.; Xu, X.; Nathanson, K. L.; Nolop, K. *Nature* **2010**, *467*, 596.
- Zamboni, A.; Menard, D.; Suijkerbuijk, B. M. J. M.; Niculescu-Duvaz, I.; Whittaker, S.; Niculescu-Duvaz, D.; Nourry, A.; Davies, L.; Manne, H. A.; Lopes, F.; Preece, N.; Hedley, D.; Ogilvie, L. M.; Kirk, R.; Marais, R.; Springer, C. J. *J. Med. Chem.* **2010**, *53*, 5639.
- Barsoum, F. F.; Hosni, H. M.; Girgis, A. S. *Bioorg. Med. Chem.* **2006**, *14*, 3929.
- De, D. Y. D.; Krogstad, F. M.; Byers, L. D.; Krogstad, D. J. *J. Med. Chem.* **1998**, *41*, 4918.
- Ghorab, M. M.; Ragab, F. A.; Alqasoumi, S. I.; Alafeefy, A. M.; Aboulmagd, S. A. *Eur. J. Med. Chem.* **2010**, *45*, 171.
- El-Gamal, M. I.; Choi, H. S.; Yoo, K. H.; Baek, D.; Oh, C. H. *Chem. Biol. Drug Des.* **2013**, *82*(3), 336.
- Hoeflich, K. P.; Herter, S.; Tien, J.; Wong, L.; Berry, L.; Chan, J.; O'Brien, C.; Modrusan, Z.; Seshagiri, S.; Lackner, M.; Stern, H.; Choo, E.; Murray, L.; Friedman, L. S.; Belvin, M. *Cancer Res.* **2009**, *69*, 3042.
- Horsman, M. R.; Siemann, D. W.; Chaplin, D. J.; Overgaard, J. *Radiother. Oncol.* **1997**, *45*, 167.
- Hoskin, P. J.; Rojas, A. M.; Saunders, M. I.; Bentzen, S. M.; Motohashi, K. J. *Radiother. Oncol.* **2009**, *91*, 120.
- Choudhury, S.; Krishna, M.; Bhattacharya, R. K. *Cancer Lett.* **1999**, *147*, 39.
- Li, C. Y.; Li, Q. S.; Yan, L.; Sun, X. G.; Wei, R.; Gong, H. B. *Bioorg. Med. Chem.* **2012**, *20*, 3746.
- Yang, Y. S.; Li, Q. S.; Sun, S.; Zhang, Y. B.; Wang, X. L.; Zhang, F. *Bioorg. Med. Chem.* **2012**, *20*, 6048.
- Li, Q. S.; Li, C. Y.; Lu, X.; Zhang, H. *Eur. J. Med. Chem.* **2012**, *50*, 288.
- Li, Q. S.; Lv, X. H.; Zhang, Y. B.; Dong, J. J.; Zhou, W. P.; Yang, Y. *Bioorg. Med. Chem. Lett.* **2012**, *22*, 6596.
- Dong, J. J.; Li, Q. S.; Wang, S. F.; Li, C. Y.; Zhao, X.; Qiu, H. Y.; Zhao, M. Y. *Org. Biomol. Chem.* **2013**, *11*, 6328.
- Boumendjel, A.; Boccard, J.; Carrupt, P.-A.; Nicolle, E.; Blanc, M.; Geze, A.; Choisnard, L.; Wouessidjewe, D.; Matera, E. L.; Dumontet, C. *J. Med. Chem.* **2008**, *51*, 2307.